https://doi.org/10.5194/acp-2020-175
Preprint. Discussion started: 16 March 2020

Atmospheric Chemistry and Physics Discussions

Determination and climatology of diurnal cycle of atmospheric mixing layer height over Beijing 2013-2018: Lidar measurements and implication for air pollution

Haofei Wang[1,2], Zhengqiang Li[1*], Yang Lv[1,2], Ying Zhang[1], Hua Xu[1], Jianping Guo[3], Philippe Goloub[4]

1. State Environmental Protection Key Laboratory of Satellite Remote Sensing, Aerospace Information Research Institute, Chinese Academy of Sciences, Beijing, 100101, China
2. University of Chinese Academy of Sciences, Beijing, 100101, China
3. State Key Laboratory of Severe Weather, Chinese Academy of Meteorological Sciences, Beijing, 100081, China
4. Laboratoire d'Optique Atmospherique, UMR8518, CNRS – Universit ´ e de Lille 1, Villeneuve d'Ascq, Lille, 59000, France

∗ *Correspondence to:* Zhengqiang Li (Email: lizq@radi.ac.cn)

Abstract. The atmospheric mixing layer height (MLH) determines the volume available for the dispersion of pollutants and thus contributes to the assessment of the pollutant concentration near the surface. The study evaluates the capability of lidar to describe the evolution of atmospheric mixing layer and then presents a long term observed climatology of MLH diurnal cycle. A system for automatic detection of the mixing layer height based on two wavelet methods (MLH and MLH') applied to lidar observations was operated from January 2013 to December 2018 in the Beijing urban area. The two dataset results are compared with radiosonde as case studies and statistical form. MLH shows good performance to calculate the convective layer height at daytime and the residual layer height at night. While MLH' has the potential to describe the stable layer height as radiosonde at night, the performance is limited due to the high range gate of lidar. A nearly six year climatology for diurnal cycle of MLH is calculated for convective and stable conditions using the dataset of MLH from lidar. The MLH characteristics of seasonal change in Beijing indicate that it is low in winter and autumn, and high in spring and summer. A significant phenomenon is found that from 2013 to 2018, the diurnal cycle of MLH increase year by year. It may partly benefit from the improvement of air quality. As to converting the column optical depth to the surface pollution, MLH from lidar shows better accuracy than that from radiosonde. Additionally, the accuracy with lidar MLH shows a diurnal cycle, with the peak at time of 1400 LST. The study provides a significant dataset of MLH based on measurement and could be an effective reference to atmospheric models for surface air pollution calculation and analysis.

1. Introduction

The height of mixing layer (MLH) is a crucial parameter for air quality forecast, pollutants dispersion and identification of pollutant emissions and sources (Haeffelin et al., 2012; Seibert et al., 2000; Liu and Liang, 2010). Pollutant emitted into the atmospheric boundary layer is gradually dispersed vertically through the action of turbulence (Gan et al., 2011; Monks et al., 2009; Guo et al, 2016), and finally becomes completely mixed over this layer if sufficient time is given (Emeis et al., 2008).

https://doi.org/10.5194/acp-2020-175
Preprint. Discussion started: 16 March 2020

Atmospheric Chemistry and Physics Discussions

The MLH determines the volume available for the dispersion of pollutants and thus contributes to the assessment of the pollutant concentration near the surface which might be harmful to people and ecosystems (Collaud et al., 2014; Emeis et al., 2007).

Within the planetary boundary layer (PBL) the height of the mixing layer (ML) is defined as the height up to which vertical dispersion by turbulent mixing of air pollutants takes place due to the thermal structure of the PBL (Seibert et al., 2000; Schafer et al., 2006; Emeis et al., 2007).MLH depends largely on the synoptic weather situation (Emeis et al., 2008). Consequently, MLH can be estimated by the measurement of mechanical turbulence, of the temperature enabling convection or of the concentration of PBL constituents. These detection approaches are based on various atmospheric parameters, various measuring instruments and different analysis algorithms, leading to several MLH estimations that are not always consistent with each other (Collaud et al., 2014).

In order to realize from the general definition to practical measurements, it is necessary to consider separately the structure of the convective boundary layer (CBL) and the stable boundary layer (SBL). In the case of fair weather days, the PBL height has a well-defined structure and diurnal cycle (Collaud et al., 2014. See Fig.S1 in the supplementary information), consisting of the development of a convective boundary layer (CBL) during the day and of a stable boundary layer (SBL), which is capped by a residual layer (RL) during the night(Stull, 1988).The PBL development under clear sky conditions that result in strong convection driven mainly by solar heating will be called CBL (Collaud et al., 2014). The nocturnal SBL presents a more complicated internal structure, which is comprised of a stable layer caused by radiative cooling from the ground and gradually merges into a neutral layer called the RL (Collaud et al., 2014; Stull, 1988; Salmond and McKendry, 2005; Mahrt et al., 1998). The RL height is the top of the neutral layer and the beginning of the stable free troposphere. The pollutants emission from the surface during the night are trapped into the SBL, whereas the pollutants released on past day tend to stay in the RL. Despite the dominance of CBL in the afternoon, the SBL and neutral boundary layer may form under certain meteorological conditions (Stull 1988; Poulos et al. 2002; Medeiros et al. 2005; Zhang et al., 2018)

Due to most of the aerosol particles in the atmospheric column are usually confined to atmospheric layers below MLH, the knowledge on MLH can thus be employed to convert column-mean optical depths measured from sunphotometer and satellite into near-surface air quality information (Sifakis et al., 1998; Emeis et al., 2007). Particles may serve as good indicator of atmospheric layering because their vertical distribution is strongly influenced by the thermal structure of the atmosphere (Neff and Coulter, 1986). Provided the vertical aerosol distribution adapts rapidly to the variational thermal-dynamic of the boundary layer, MLH can thus be retrieved from the analysis of this aerosol distribution（Emeis et al., 2008）.

By the measurement of profile of aerosol, lidar offers a direct and continuous way to monitor the diurnal cycle of the different layers constituting the PBL (Seibert et al., 2000; De Haij et al., 2006;Emeis et al., 2008;. Liu and Liang 2010; Tang et al, 2016; Su et al, 2017, 2019). Recent studies compared lidar techniques with radiosonde (RS) measurements (Milroy et al., 2012;

https://doi.org/10.5194/acp-2020-175
Preprint. Discussion started: 16 March 2020

Atmospheric Chemistry and Physics Discussions

Sawyer and Li, 2013; Cimini et al., 2013; Tang et al, 2016; Su et al, 2019), of which good correlations are found in the case of convective weather conditions with differences of 100–300 m, while non-convective weather conditions lead to much larger difference in the MLH estimations. In these cases, the discrepancy tends to be even larger if the approaches are supposed to measured different structure of ML such as CBL, SBL or RL (Collaud et al., 2014). The meteorological radiosondes can only acquire the MLH in the morning (08:00 LT) and at night (20:00 LT), when the ML tends to be stable and the convective condition is lacking. Ceilometer is used to measure the diurnal variation of MLH, however, the accuracy suffers from its low vertical resolution and poor signal noise ratio (De Haij et al., 2006; Tang et al., 2016). Su et al. (2019) indicates that lidar shows good consistent with RS in the daytime stable condition with the improved algorithm, but the nocturnal MLH with very low SBL height is not evaluated.

In the existing studies, numerical simulations, ground-based remote sensing, or meteorological radiosonde are used to obtain the characterization of MLH during short time periods in Beijing, mainly focusing on heavy pollution event (Yang et al., 2005; Zhang et al., 2006; Quan et al., 2013; Hu et al., 2014; Zhang et al., 2015), which underscores the scarceness of continuous high-resolution observations for a long time period. Depending on the measured atmospheric parameters and observational uncertainties, different measurement approaches may reveal different aspects of PBL structure (Seibert et al., 2000; Seidel et al., 2010; Beyrich and Leps, 2012). Thus, it is of great significance to apply consistent algorithm to consistent types of atmospheric structure parameter when comparing MLH from different times.

The main objective of this study, therefore, is aimed to present a long term observed climatology of the MLH diurnal cycle based on lidar observations. For that, the capability of lidar to describe the diurnal evolution of mixing layer height is evaluated first. The data and methods used are described in Section 2. Sect. 3 is the result and discussion, which consist of the comparison of lidar-derived MLH with radiosonde measurements, the climatology of MLH in Beijing and implication for surface pollution retrieval. Then, it is concluded in Sect. 4.

2. Data and methods

2.1. Site and lidar measurements

In the study, the observation site (116.37 ° E, 40.00 ° N) in Beijing city is located on the building roof (59 m a.s.l.) of the Institute of Remote Sensing and Digital Earth, Chinese Academy of Sciences. The micro pulse lidar (CE370, CIMEL, France) was used at wavelength of 532nm with the vertical resolution of 15 m. The laser used is frequency-doubled Nd:YAG with pulse repetition frequency 4.7 kHz and energy 8-20 μJ. The signal received from lidar is processed by subtraction of atmospheric background, correction of overlap, correction of range (range corrected signal, RCS), and then logarithm calculation (expressed in In(β'_{532})) (Yan et al., 2014; Campbell t al. 2003； Su et al., 2019). MLH estimation from lidar systems is based on the detection of the sharp decrease in aerosol backscatter at the top of the mixing layer (Seibert et al., 2000) .

https://doi.org/10.5194/acp-2020-175
Preprint. Discussion started: 16 March 2020

Atmospheric Chemistry and Physics Discussions

2.2. MLH derived from Lidar

Wavelet transforms are commonly used in many studies for MLH determination from lidar observations (Cohn and Angevine, 2000; Davis et al., 2000; Brooks, 2003; De Haij et al., 2006; Su et al., 2019). When it is the maximum value of attenuated backscattering profile convolved with Haar function, the corresponding height is MLH. The equation of wavelet is defined as follows:

$$h\left(\frac{z-b}{a}\right)=\begin{cases}1, & b-\frac{a}{2}\le z\le b;\\ -1, & b<z\le b+\frac{a}{2}\\ 0, & else\end{cases} \quad (1)$$

Where b is the transformation of the equation, where the equation is cantered, and a is the expansion of the equation. The equation of wavelet covariance transformation $W_f(a,b)$, namely, the convolution of attenuated backscattering profile f(z) with wavelet function is defined as follows:

$$W_f(a,b)=\frac{1}{a}\int_{z_b}^{z_t} f(z)h\left(\frac{z-b}{a}\right)dz \quad (2)$$

Where f(z) represents the backscatter signal of lidar, z_b denotes the lower limit of the height of the profile, and z_t represents the upper limit of the height. A valid MLH is detected corresponding to the value b when W_f (a, b) reaches the biggest local maximum with a coherent scale of a (Brooks, 2003; De Haij et al., 2006; Emeis et al., 2008). In this study, the expansion a is selected as 420 m, 435 m, 450 m, respectively, and final W_f (a, b) is calculated from the averaged corresponding values. Another layer, named MLH' is detected simultaneously by the first local maximum W_f (a, b) from z_b, which is assumed to be smaller than or equal to MHL (De Haij et al., 2006). Since the absolute maximum in the vertical gradient of the lidar profiles is characterized by the rapid degrease in pollutants concentration, the MLH can be associated with the CBL height during day and to the RL during night (Collaud et al., 2014). However, the detection of MLH' is used to try to detect the height of SBL in the nocturnal time.

The scheme of cloud screen follows that MLH is eliminated if a cloud flag is marked when the cloud base is found within 6 km from the surface. Due to the limitation of algorithm and insufficient lidar overlap, the MLH calculation starts from 255 m. All MLH results are one hour averaged and processed under good quality control, which involves with elimination of incomplete data, false value and peak value, and so on.

2.3. MLH from Radiosonde

Radiosonde is usually considered as the ground truth for the detection of CBL height at daytime and SBL height at nocturnal time. The meteorological radiosondes (RS) are measured at the international standard weather station (39.484 °N, 116.282 °E), where was located nearly 11 km far from lidar station. It includes two categories: conventional observations around the year, which are performed at 0000 UTC (0800 LST) in the morning and at 1200 UTC (2000 LST) in the evening each day;

https://doi.org/10.5194/acp-2020-175
Preprint. Discussion started: 16 March 2020

and intensified observations only in summer, which are operated at 0600 UTC (1400 LT) in the afternoon. The observed meteorological parameters includes atmospheric pressure (P), temperature (T), relative humid (RH), wind speed (WS), wind direction (WD), and so on.

The bulk Richardson number (Ri_b) is a dimensionless parameter combining the thermal energy and the vertical wind shear, and is widely used in MLH climatology (Seidel et al., 2012; Collaud et al., 2014). R_i is defined as the ratio of turbulence associated with buoyancy to that induced by mechanical shear, which is expressed as

$$Ri_b = \frac{gz(\theta(z)-\theta(z_s))}{\theta_{z_s}(U^2(z)+V^2(z))} \quad (3)$$

where z is the height ($z > z_s$, subscript 's' denote the surface), θ characters virtual potential temperature, U and V indicates the two horizontal wind velocity components, g presents the Earth gravitational constant. The MLH corresponds to the first elevation z with Ri_b greater than a critical threshold taken as 0.25 (Stull, 1988; Seidel et al. 2012; Guo et al., 2016, 2019). In most cases, the exact threshold value has only a small impact on the PBL height due to the large slope of Ri_b in this interval (Collaud et al., 2014).

2.4 Air pollution model

The data of MLH is usually combined within the atmospheric model to obtain the surface air pollutant concentration. For example, $PM_{2.5}$ remote sensing（PMRS）model, derived by Zhang and Li (2015), have the ability to calculate the mass concentration of $PM_{2.5}$ above ground. The PMRS method is designed to employ currently available remote sensing parameters, including aerosol optical depth (AOD), fine mode fraction (FMF), planetary boundary layer height (PBLH) and atmospheric relative humidity (RH), to derive $PM_{2.5}$ from instantaneous remote sensing measurements under different pollution levels(Zhang and Li, 2015; Li et al., 2016;Yan et al., 2017, detail information see S2). In this study, AOD and FMF is retrieved by a sunphotometer located with the lidar, while RH is measured by a meteorology station in the same station. The MLH obtained both from lidar and radiosonde is used in the model to calculate the surface $PM_{2.5}$.

3. Results and Discussions

3.1. MLH operational measurement: case study

A selection of typical atmospheric conditions included in the data set of lidar measurement are plotted in Fig. 1 - Fig. 4. The heights of the mixing layer (MLH and MLH') are obtained from different criteria using the wavelet covariance transform method. As shown in Fig.1, the development of a convective mixing layer could clearly be observed, with a sharp decrease in aerosol backscatter between the mixing layer and the free atmosphere. In the fair weather, there should be an obvious diurnal variation in the height of the boundary layer, which gradually rises at 8 am, reaches a maximum at 2 - 3 pm, and gradually decreases at night. This is related to the diurnal change of the surface radiation, which is the driving factors of boundary layer.

https://doi.org/10.5194/acp-2020-175
Preprint. Discussion started: 16 March 2020

Atmospheric Chemistry and Physics Discussions

However, in fact, the MLH from lidar is sometime not consist with thermodynamics PBL height, which could be obtained by MLH_RS (MLH from radiosonde) indicated by the dramatic variance of relative humidity (RH) and temperature (T). When the PBL reaches the top and the thermodynamics PBL starts to decrease, the aerosol layer height keep for still or sometime even grow for some distance, rather than going down immediately, just as Fig.1a shown. MLH is always higher than MLH_RS, which indicates the stable layer height at 2000 LST. It should be noted that above the MLH_RS there still exist abundance of aerosols. The aerosol layer height should be the top of residual layer height, which corresponds to MLH at nocturnal time, determined by the greatest gradient of aerosol concentration.

In some cases, the result of MLH', present by first local maximal aerosol gradient, agree well with MLH_RS. Sometime in the evening and early morning MLH' deviated from MLH and approached to MLH_RS, as shown as the vertical profile of lidar and radiosonde at 2000 (LST) of 20170303(Fig.1b). Fig.1c shown that MLH' approaches to MLH_RS, albeit a little higher, and much lower than MLH. However, MLH' would not always correspond to MLH_RS, just like Fig.1d. MLH' (0.752 km) is much higher than MLH_RS (0.243 km), but equal to MLH. It is related to that the stable layer height obtained from radiosonde in the case is out of the range of lidar detection (0.255 km), in which, that is, MLH' from lidar is disabled to determine the stable layer height.

In the summer time (JJA) when the radiosonde is additionally launched at 1400 LST to detect the convective boundary layer, MLH is consistent with MLH_RS, while MLH' is frequently under MLH_RS, as shown in Fig.2. The detailed information represented in Fig.2b shows that MLH is equal to MLH_RS, which reaches up to 2.95km, while MLH' is only 1.24km. Under clear sky conditions, problems in estimating the MLH from lidar data can arise from the weak vertical gradients in the aerosol content as indicated by RCS. Fig.2c and 2d indicate that MLH approaches to MLH_RS, but a little lower than MLH_RS. The difference is associated with that aerosol within the mixing layer needs some time to adjust the thermal structure, and exist a delay to reach the thermodynamics MLH (Stull, 1988; Collaud et al., 2014).

As fig.3 shown that MLH' corresponds to MLH_RS for most time. But when stable layer height was around 0.25 km, both MLH' missed the height of SBL, but point to the height of residual layer (Fig.3b. and Fig.4).When stable layer height is higher than 0.25 km, MLH' tend to approach to MLH_RS (Fig.3d.). However, in the afternoon MLH was used to be close to MLH_RS than MLH' (Fig.3c.). In some synoptic condition, the PBL stays stable in the whole day,and the height of SBL is missed by MLH' (Fig.4).

The greatest advantage of PBL detection by RS is its very good precision. However, radiosonde, crossing the PBL along a slanted path within a few minutes, provides only a "snapshot"-like profile (Seibert et al., 2000). Its temporal resolution (two or three measurements per day) is not able to provide the MLH diurnal cycle. Meanwhile, radiosonde detects the daytime and nighttime layers in which ground-emitted atmospheric pollutants are trapped, but not the residual layer height corresponding to trapped atmospheric constituents discharged some hours before (Collaud et al., 2014).

https://doi.org/10.5194/acp-2020-175
Preprint. Discussion started: 16 March 2020


Atmospheric Chemistry and Physics Discussions

As for lidar measurement, MLH tends to obtain CBL height in the afternoon and RL height at night and early morning. MLH' sometime agree well with SBL height in nocturnal time and early morning, and it has the potential to describe the SBL. However, MLH' is disabled in the case that SBL height is out of lidar measurement gate. And, in the afternoon, MLH' is frequently lower than CBL height. Therefore, for the operational lidar measurement of PBL height, MLH is more suitable and has the capability to mark the diurnal circle of mixing layer height. Hence, MLH obtained by the lidar can be used as an effective parameter for the vertical distribution of aerosols, and provides an important reference to obtain near-ground pollutant concentrations for atmospheric model.

3.2. Inter-comparison of different MLH approaches

A comparison of MLH estimated by lidar and radiosonde profiles of 0800 and 2000 LST, were shown in Figure 5. The same observation period of nearly six year (2003-2008) was considered, among them for 2013 only the month of 1-4 and 11-12. As shown in the histograms of Fig.5, there is a wide discrepancy between MLH and MLH_RS at the time of 0800 and 2000 LST. The frequency of MLH from radiosonde lower than 0.25 km is nearly 35%， where it is no data for MLH from lidar due to the limited detection range. Specifically, the rate of MLH from lidar smaller than 0.5 km is nearly 18% and 12%,repectively,at 0800 LST and 2000 LST, while the corresponding frequency of radiosonde is beyond 75% and 66%. The frequency of larger MLH value at the time of 2000 LST is bigger than that of 0800 LST, both from lidar and radiosonde. It is reasonable that the residual layer have not yet collapse entirely at 2000 LST, while the CBL have not develop well in the early morning. As for the MLH', its distribution trend is more similar to MLH_RS than MLH (See Fig.S3), and that the correlation between MLH' and MLH_RS is higher than that between MLH and MLH_RS, in spite that it is still not good (See Fig.S4). It indicates once again that MLH' have the potential to determine the SBL height as radiosonde does. As to the seasonal variation of both lidar and RS measurement at 0800 LST, the frequency of larger MLH value in summer is minimal, indicating summer MLH is lower than other season. As for radiosonde, MLH lower than 0.25 km most distributes in winter, with the rate of around 15% for both 0800 and 2000 LST, and the frequency decreases rapidly when MLH gets larger than 0.25 km.

The comparison of MLH and MLH_RS at time of 1400 LST in summer is presented in Fig.6, both of them mainly indicating the CBL height. MLH shown very good agreement with MLH_RS, with correlation coefficient of 0.692 and RMSE of 0.573 km. It is noted that the slope of linear fitting line is smaller than 1:1 line, indicating that MLH_RS tends to be larger than MLH, which is consistent with the case study. Although the comparison only exist in summer, it can be generally concluded that MLH from lidar in the afternoon characters the CBL height with good accuracy.

In fact, it would not exist complete agreement between MHL values derived from lidar and radiosonde associated with several reasons. First, the two systems measure different atmospheric parameters (aerosol for lidar and temperature, humidity, wind for radiosonde) with varying height resolution and accuracy. Furthermore, vertical profiles of these parameters are influenced in different way by the processes occurring within PBL, including radiation, convection, subsidence, advection, heating and

https://doi.org/10.5194/acp-2020-175
Preprint. Discussion started: 16 March 2020


Atmospheric Chemistry and Physics Discussions

cooling, gravity waves. It is almost impossible to separate the various contributions to the observed PBL structure (Seibert et al., 2000). Additionally, it is difficult to identify a clear upper boundary of the mixing layer because the measured parameter (MLH) is actually not a fixed point but rather a transition layer between two atmospheric states (Stull, 1988; Garratt, 1992; Collaud et al., 2014).

3.3. Climatology of MLH in Beijing

3.3.1. Diurnal cycle

A data set containing nearly six years measurement in Beijing is used for assessment of the overall performance of the Wavelet MLH algorithm (MLH and MLH') with respect to the diurnal availability, as shown in Fig. 7. It can be seen that the expected shape resembling the growth of a convective mixing layer is observed. The diurnal cycles derived from MLH match well with RS results in the afternoon, but larger than MLH_RS in the early morning and evening. Contrarily, MLH' tend to approach to MLH_RS in the early morning and evening, but keep away from MLH_RS in the afternoon.

Owing to solar heating of the surface, when convective layer begin to rise due to upward convection in the early morning and nocturnal residual layer tends to collapse, MLH from lidar presents the minimal value. After that, MLH grows continuously and reaches its maximum height around 1500 (Stull et al., 1984; Tang et al, 2016; Su et al, 2019). The difference between MLH and MLH_RS at 1400 is less around 0.1 km. It is reasonable considering that RS data is acquired at 1400 only from summer time, when MLH is usually larger around the year. However, MLH is nearly 0.46 km larger than MLH' throughout the day, and with bigger standard deviation. The nocturnal SBL top is defined as the transition between the stable surface layer and the residual layer (Stull, 1988; Collaud et al, 2014).Although MLH' can catches the high SBL height, due to lidar usable range gate, the point derived from MLH' is residual layer height rather than the nocturnal SBL height. As a contrast, MLH retrieve the consistent RL height during the night following the CBL diurnal maximal. And, the SBL height provided by radiosonde at 0800 and 2000 LST can be considered as complementary to the lidar approaches.

3.3.2. Seasonal variation

The seasonal mean diurnal cycle of the MLH from lidar are shown in Figure 8. An evident seasonal variation of magnitude of the diurnal cycle is observed. The smallest MLH magnitude is found in winter with the peak value of 1.40 km at 1500 LST, whereas spring demonstrates the maximum magnitude with 1.64 km at 1500 LST. It should be noted that summer exists the biggest amplitude of diurnal variation, with the deepest valley (0.93 km) increasing to the peak value of 1.51 km. As the statistic variation, the values of autumn MLH vary most nearly at each hour with the bigger standard deviation, indicating the great fluctuations in the long measurement period, while variation of summer MLH values for most hour is relative stable.

Previous studies have suggested that the seasonal variation in the MLH may be associated with radiation flux (Stull, 1988; Kamp and McKendry, 2010; Munoz and Undurraga, 2010), which was consistent with our results. The larger MLH in spring

https://doi.org/10.5194/acp-2020-175
Preprint. Discussion started: 16 March 2020


Atmospheric Chemistry and Physics Discussions

than that in summer can be explained by the higher total radiation flux than summer. The relatively low values in autumn and winter are likely to related to the low radiation flux. Tang et al. (2016) revealed the similar seasonal variation in Beijing, which is that the MLH is low in autumn and winter, and high in spring and summer. For the lowest MLH in the early morning of summer, a possible explanation may be that the strong convective mixing, due to intense strong surface heating, leads to the greatest aerosol gradient forming at the top of convective boundary layer, rather than that of residual layer in the early morning.

3.3.3. Interannual variation

Interannual variations of MLH diurnal cycle are investigated in Beijing from 2013 to 2018. As shown in Fig. 9, diurnal variations of MLH in different years all have same patterns, but with the different magnitude. Clearly, from 2013-2018, the values of diurnal circle MLH increase year by year, including both the RL height at night and CBL height at daytime. Since the data of 2013 is mainly from winter and spring, the MLH seems stable, not like the amplitude of other years. Increment of nearly 400 m is found between 2014 and 2018. The amplification of MLH between 2014 and 2016 is larger than that of 2016-2018, while the MLH value of 2016 and 2017 is very close.

In addition to the effects of meteorological conditions (Wang et al., 2017), the increase of the MLH may benefit from the improvement of air quality in Beijing in recent years. The estimated national population–weighted annual average $PM_{2.5}$ concentrations declined from 61.8 to 42.0 μg/m^3 from 2013 to 2017 (Zhang et al., 2019). Due to the relief of radiation effect by aerosol, the turbulence increases, thus leading to larger MLH (Ding et al., 2016; Li et al., 2017; Wang et al., 2019).

3.4. Implication for surface pollution retrieval

The dataset of MLH from lidar is able to indicate the height of the aerosol layer throughout the whole day. Thus, the knowledge on MLH can be employed to convert column-mean optical depths into near-surface air quality information (Sifakis et al., 1998; Dandou et al., 2002; Schafer et al., 2008). Using MLH data and other aerosol related parameters, the mass concentration of $PM_{2.5}$ above ground is calculated based the PMRS model. Due to the difference in the source of the MLH, lidar and radiosonde, the comparison of derived $PM_{2.5}$_lidar and $PM_{2.5}$_RS with the in-situ observational $PM_{2.5}$ data at 0800 LST is presented in Fig. 10a and 10b. MLH from lidar shows reasonably good performance for the retrieval of $PM_{2.5}$ in the morning, with the correlation coefficients of 0.741 and RMSE 46.69 ug/m^3. However, the calculated $PM_{2.5}$ from MLH_RS obviously overestimate the surface pollution, with lower correlation coefficients and larger standard deviation. The large overestimation should be due to the underrating of aerosol layer height. In the morning, MLH_RS is the height of the SBL, above which there still exist some amount of aerosol. Therefore, MLH from lidar, as the good indicator of the aerosol layer height, is more suitable for estimating the surface air pollution from the column-mean optical depths.

As presented in Fig.10c, the calculated $PM_{2.5}$_lidar data of daytime period (0800-1700 LST) shows better accuracy than that of only the early morning. Actually, the accuracy also shows a diurnal cycle, with the peak of correlation coefficients (0.927)

https://doi.org/10.5194/acp-2020-175
Preprint. Discussion started: 16 March 2020

Atmospheric Chemistry and Physics Discussions

at 1400 LST (Fig.10d). The high accuracy could lead from aerosol mixing well at noon time, while the relative poor accuracy is related with the complicate layers in the early morning and at dusk. Based on the observational data, $PM_{2.5}$ tends to peak in the morning and evening. In contrast, afternoon usually witnessed lower mass concentration due to rapid vertical diffusion of aerosols (Guo et al., 2016).Thus, MLH from lidar can offer the significant contribution to retrieve the diurnal circle of the surface air pollution. Additionally, the existing diurnal cycle of MLH data sets from ground-based lidar can facilitate effective analysis of current space-borne lidar missions and to support new space lidar mission around the topic of atmospheric environment at different measurement time.

4. Conclusion

To acquire the high-resolution observations of MLH diurnal variation, a study using lidar was performed from January 2013 to December 2018 in the Beijing urban area. For this study a system for automatic detection of the ML height based on two wavelet methods (MLH and MLH') applied to lidar observations is operated. The two data results are compared with radiosonde as case studies and statistical forms. MLH shows good performance for the convective layer height at daytime and the residual layer height at night. MLH' have the potential to describe the stable layer height at night sometime, but due to the high range gate of lidar, the performance is limited. Nevertheless, it could be a useful complementary as stable layer height for dataset of MLH in some cases. And, MLH' does not always work out to catch the convective layer height as MLH in the afternoon.

Nearly six year climatology for MLH diurnal cycle is calculated for convective and stable conditions. It is true that the height of the aerosol layer obtained by different approaches may be different. We focus on the temporal change of aerosol layer height with a consistent method using the dataset of MLH. The MLH characteristics of seasonal change in Beijing indicate that it is low in winter and autumn, and high in summer and spring. A significant phenomenon is found that from 2013 to 2016, the diurnal cycle of MLH increased year by year, which may partly be contributed from the improvement of air quality. As to converting the column aerosol optical depth to the surface pollution, MLH from lidar shows better accuracy than that from radiosonde. Additionally, the accuracy with lidar MLH shows a diurnal cycle, with the peak at time of 14 LST.

Actually, interpreting data from aerosol lidar is often not straightforward, because the detected aerosol layers are not always the result of ongoing vertical mixing, but may originate from advective transport or past accumulation processes (Russell et al., 1974; Coulter, 1979; Baxter, 1991; Batchvarova et al., 1999). Each detection method has good performances only for defined ML structures and under specific meteorological conditions. Therefore, only the combination of several methods and instruments allows one to follow the complete diurnal cycle of the complex ML structure.

https://doi.org/10.5194/acp-2020-175
Preprint. Discussion started: 16 March 2020

Atmospheric Chemistry and Physics Discussions

References

Barbaro E , J. Vil à-Guerau de Arellano, Krol M C , et al. Impacts of Aerosol Shortwave Radiation Absorption on the Dynamics of an Idealized Convective Atmospheric Boundary Layer. Bound.-Lay. Meteorol., 2013, 148(1):31-49.

Batchvarova, E., Cai, X., Gryning, S.E., Steyn, D., 1999. Modelling internal boundary layer development in a region with complex coastline. Boundary-Layer Meteorology 90,1-20.

Baxter, R.A., 1991. Determination of mixing heights from data collected during the 1985 SCCCAMP field program. Journal of Applied Meteorology 30, 598-606.

Bbooks, I.M., 2003: Finding boundary layer top: application of a wavelet covariance transform to lidar backscatter profiles. J. Atmos. Oceanic. Technol. 20, 1092–1105.

Beyrich F , Leps J P . An operational mixing height data set from routine radiosoundings at Lindenberg: Methodology[J]. Meteorologische Zeitschrift, 2012, 21(4):337-348.

Campbell, J.R., Welton, E.J., Spinhirne, J.D., Ji, Q., Tsay, S.C., Piketh, S.J., Barenbrug, M.,Holben, B.N., 2003. Micropulse lidar observations of tropospheric aerosols over northeastern South Africa during the ARREX and SAFARI 2000 dry season experiments.J. Geophysics. Res. Atmos. 108.

Cimini, D., De Angelis, F., Dupont, J.-C., Pal, S., and Haeffelin, M.: Mixing layer height retrievals by multichannel microwave radiometer observations, Atmos. Meas. Tech. Discuss., 6, 4971–4998, doi:10.5194/amtd-6-4971-2013, 2013.

Cohn, S.A., W.M. Angevine, 2000: Boundary Layer Height and Entrainment Zone Thickness Measured by Lidars and Wind-Profiling Radars. J. Appl. Meteor. 39,1233–1247.

Collaud Coen M, Praz C, Haefele A, et al. Determination and climatology of the planetary boundary layer height above the Swiss plateau by in situ and remote sensing measurements as well as by the COSMO-2 model. Atmos. Chem. Phys., 14,23(2014-12-11), 2014, 14(23): 13205-13221.

Coulter, R.L., 1979. A comparison of three methods for measuring mixing layer height. Journal of Applied Meteorology 18, 1495-1499.

Dandou, A., E. Bossioli, M. Tombrou, N. Sifakis, D. Paronis, N. Soulakellis, D. Sarigiannis, 2002: The importance of mixing height in characterizing pollution levels from aerosol optical thickness derived by satellite. Water Air Soil Poll. Focus 2, 17–28.

Davis, K.J., N. Gamage, C.R. Hagelberg, C. Kiemle, D.H. Lenschow, P.P. Sullivan, 2000: An objective method for deriving atmospheric structure from airborne lidar observations. J. Atmos. Oceanic. Technol. 17, 1455–1468.

De Haij, M., W. Wauben, H. Klein Baltink, 2006: Determination of mixing layer height from ceilometer backscatter profiles. Proceedings of SPIE - The International Society for Optical Engineering, 2006, 6362.

https://doi.org/10.5194/acp-2020-175
Preprint. Discussion started: 16 March 2020

Ding, A. J., Huang, X., Nie, W., Sun, J. N., Kerminen, V. M., Petäjä, T., et al. (2016). Enhanced haze pollution by black carbon in megacities in China. Geophys. Res. Lett., 43(6), 2873–2879. https://doi.org/10.1002/2016GL067745.

Emeis, S., C. Jahn, C. Munkel, C. Munsterer, K. Schäfer, 2007: Multiple atmospheric layering and mixing-layer height in the Inn valley observed by remote sensing. – Meteorol. Z. 16, 415–424.

Emeis, S., Schäfer, K., and Münkel, C.: Surface-based remote sensing of the mixing-layer height – a review, Meteorol. Z., 17, 621– 630, 2008.

Gan, C.M., Wu, Y.H., Madhavan, B.L., Gross, B., Moshary, F., 2011. Application of active optical sensors to probe the vertical structure of the urban boundary layer and assess anomalies in air quality model PM2.5 forecasts. Atmos. Environ. 45, 6613–6621.

Garratt, J. R., 1992: The Atmospheric Boundary Layer. Cambridge University Press, 316 pp.

Guo J, Miao Y, Zhang Y, et al. The climatology of planetary boundary layer height in China derived from radiosonde and reanalysis data. Atmos. Chem. Phys., 2016, 16(20):13309-13319.

Guo J, Xia F, Zhang Y, et al. Impact of diurnal variability and meteorological factors on the PM2.5 - AOD relationship: Implications for PM2.5 remote sensing. Environ. Pollut., 2017, 221(94):94.

Guo, J., Li, Y., Cohen, J. B., Li, J., Chen, D., Xu, H., et al. (2019). Shift in the temporal trend of boundary layer height in China using long - term (1979–2016) radiosonde data. Geophysical Research Letters, 46, 6080–6089. https://doi.org/10.1029/2019GL082666

Haeffelin, M., Angelini, F., Morille, Y., Martucci, G., Frey, S., Gobbi, G.P., Lolli, S.,O'Dowd, C.D., Sauvage, L., Xueref-Remy, I., Wastine, B., Feist, D.G., 2012. Evaluation of mixing-height retrievals from automatic profiling lidars and ceilometers in view of future integrated networks in europe. Boundary-Layer Meteorol. 143, 49–75.

Hu, X., Ma, Z., Lin, W., Zhang, H., Hu, J., Wang, Y., Xu, X., Fuentes, J. D., and Xue, M.: Impact of the Loess Plateau on the atmospheric boundary layer structure and air quality in the North China Plain: a case study, Sci. Total Environ., 499, 228–237, doi:10.1016/j.scitotenv.2014.08.053, 2014.

Kamp, D. and McKendry, I.: Diurnal and seasonal trends in convective mixed-layer heights estimated from two years of continuous ceilometer observations in Vancouver, BC, Bound.-Lay. Meteorol., 137, 459–475, 2010.

Lammeret, A., J. Bosenberg , 2006: Determination of the Convective Boundary-Layer Height with Laser Remote Sensing. Bound.-Lay. Meteor. 119, 159–170.

Li, Z. Q., Guo, J. P., Ding, A. J., Liao, H., Liu, J. J., Sun, Y. L., et al. (2017). Aerosol and boundary-layer interactions and impact on air quality. National Science Review, 4(6), 810–833. https://doi.org/10.1093 /nsr/nwx117.

Li, Z., Zhang, Y., Shao, J., et al., 2016. Remote sensing of atmospheric particulate mass of dry PM2.5 near the ground: Method validation using ground-based measurements. Remote Sensing of Environment, 173, 59-68.

https://doi.org/10.5194/acp-2020-175
Preprint. Discussion started: 16 March 2020

Atmospheric Chemistry and Physics Discussions

Liu, S., and X.-Z. Liang, 2010: Observed diurnal cycle climatology of planetary boundary layer height. J. Climate, 23, 5790–5809, https://doi.org/10.1175/2010JCLI3552.1.

Mahrt, L., Sun, J., Blumen, W., Delany, T., and Oncley, S.: Nocturnal boundary-layer regimes, Bound.-Lay. Meteorol., 88, 255–278, 1998.

Martucci, G., Matthey, R., Mitev, V., and Richner, H.: Comparison between backscatter lidar and radiosonde measurements of the diurnal and nocturnal stratification in the lower troposphere, J. Atmos. Ocean. Technol., 24, 1231–1244, 2007.

Medeiros, B., A. Hall, and B. Stevens, 2005: What controls the mean depth of the PBL? J. Climate, 18, 3157–3172, https://doi.org/10.1175/JCLI3417.1.

Miao Y, Liu S, Guo J, et al. Unraveling the relationships between boundary layer height and PM2.5 pollution in China based on four-year radiosonde measurements. Environ. Pollut., 2018, 243:1186-1195.

Milroy, C., Martucci, G., Lolli, S., Loaec, S., Sauvage, L., Xueref-Remy, I., Lavrič, J. V., Ciais, P., Feist, D. G., Biavati, G., and O'Dowd, C. D.: An Assessment of Pseudo-Operational Ground-Based Light Detection and Ranging Sensors to Determine the Boundary-Layer Structure in the Coastal Atmosphere, Advances in Meteorology, 18 pp., doi:10.1155/2012/929080, 2012.

Monks, P.S., Granier, C., Fuzzi, S., et al., 2009. Atmospheric composition change - global and regional air quality. Atmos. Environ. 43, 5268–5350.

Munoz, R. C. and Undurraga, A. A.: Daytime mixed layer over the Santiago Basin: Description of two years of observations with a lidar ceilometer, J. Appl. Meteorol. Clim., 49, 1728–1741,2010.

Neff, W.D., R.L. Coulter, 1986: Acoustic remote sensing. Probing the Atmospheric Boundary Layer. – In: D.H. LENSCHOW (Ed.), Amer. Meteor. Soc. Boston, MA, 201–239.

Poulos, G. S., and Coauthors, 2002: CASES-99: A comprehensive investigation of the stable nocturnal boundary layer. Bull. Amer. Meteor. Soc., 83, 555–581, https://doi.org/10.1175/1520-0477(2002)083,0555.

Quan, J., Gao, Y., Zhang, Q., Tie, X., Cao, J., Han, S., Meng, J., Chen, P., and Zhao, D.: Evolution of planetary boundary layer under different weather conditions, and its impact on aerosol concentrations, Particuology, 11, 34–40, doi:10.1016/j.partic.2012.04.005, 2013.

Russell, P.B., Uthe, E.E., Ludwig, F.L., Shaw, N.A., 1974. A comparison of atmospheric structure as observed with monostatic acoustic sounder and lidar techniques. Journal of Geophysical Research 79, 5555-5566.

Salmond, J. A. and McKendry, J. A.: A review of turbulence in the very stable nocturnal boundary layer and its implications for air quality, Prog. Phys. Geog., 29, 171–188, 2005.

Sawyer, V. and Li, Z.: Detection, variations and intercomparison of the planetary boundary layer depth from radiosonde, lidar and infrared spectrometer, Atmos. Environ., 79, 518–528, 2013.

Schafer, K., S. Emeis, H. Hoffmann, C. Jahn, 2006: Influence of mixing layer height upon air pollution in urban and sub-urban area. Meteorol. Z. 15, 647-658. DOI:10.1127/0941-2948/2006/0116.

Seibert, P., Beyrich, F., Gryning, S.E., Joffre, S., Rasmussen, A., Tercier, P., 2000. Review and intercomparison of operational methods for the determination of the mixing height. Atmos. Environ. 34, 1001–1027.

Seidel, D. J., Ao, C. O., & Li, K. (2010). Estimating climatological planetary boundary layer heights from radiosonde observations: Comparison of methods and uncertainty analysis. Journal of Geophysical Research, 115, D16113. https://doi.org/10.1029/2009JD013680

Seidel, D. J., Zhang, Y., Beljaars, A., Golaz, J. - C., Jacobson, A. R., & Medeiros, B. (2012). Climatology of the planetary boundary layer over the continental United States and Europe. Journal of Geophysical Research, 117, D17106. https://doi.org/10.1029/2012JD018143

Sifakis, N., N. Soulakellis, D. Paronis, 1998: Quantitative mapping of air pollution density using Earth observations: a new processing method and application to an urban area. – Intern. J. Rem. Sens. 19, 3289–3300.

Stull, R. B., 1988: An Introduction to Boundary Layer Meteorology. Kluwer Academic, 666 pp.

Su, T., J. Li, C. Li, P. Xiang, A. K.-H. Lau, J. Guo, D. Yang, and Y. Miao (2017), An intercomparison of long-term planetary boundary layer heights retrieved from CALIPSO, ground-based lidar, and radiosonde measurements over Hong Kong, J. Geophys. Res.-Atmos., 122, doi:10.1002/2016JD025937.

Su, T., Z. Li, and R. Kahn, 2019: A new method to retrieve the diurnal variability of planetary boundary layer height from lidar under different thermodynamic stability conditions, Remote Sens. Environ., 237, doi:10.1016/j.rse.2019.111519.

Tang, G., Zhang, J., Zhu, X., Song, T., Münkel, C., Hu, B., Schäfer, K., Liu, Z., Zhang, J., Wang, L., Xin, J., Suppan, P., and Wang, Y.: Mixing layer height and its implications for air pollution over Beijing, China, Atmos. Chem. Phys., 16, 2459–2475, https://doi.org/10.5194/acp-16-2459-2016, 2016.

Wang H. F., Li Z. Q., Lv Y., et al., Observational study of aerosol-induced impact on planetary boundary layer based on lidar and sunphotometer in Beijing, Environmental Pollution, 252, 897-906, 2019. https://doi.org/10.1016/j.envpol.2019.05. 070.

Wang, X., Dickinson, R. E., Su, L., Zhou, C., and Wang, K.: PM2.5 pollution in China and how it has been exacerbated by terrain and meteorological conditions, B. Am. Meteorol. Soc., https://doi.org/10.1175/BAMS-D-16-0301.1, 2017.

Yan, H.R., Li, Z.Q., Huang, J.P., Cribb, M., Liu, J.J., 2014. Long-term aerosol-mediated changes in cloud radiative forcing of deep clouds at the top and bottom of the atmosphere over the Southern Great Plains. Atmos. Chem. Phys. 14, 7113–7124.

Yan, X., Shi, W., Li, Z., Li, Z., Luo, N., Zhao, W., Wang, H., Yu, X., Satellite-based PM2.5 estimation using fine-mode aerosol optical thickness over China, Atmospheric Environment (2017), doi: 10.1016/j.atmosenv.2017.09.023.

Yang, H., Liu, W., Lu, Y., Xie, P., Xu, L., Zhao, X., Yu, T., and Yu, J.: PBL observations by lidar at Peking, Optical Tech., 31,221–226, 2005.

https://doi.org/10.5194/acp-2020-175
Preprint. Discussion started: 16 March 2020

Zhang, Q., Quan, J., Tie, X., Li, X., Liu, Q., Gao, Y., and Zhao, D.: Effects of meteorology and secondary particle formation on visibility during heavy haze events in Beijing, China, Sci. Total Environ., 502, 578–584, doi:10.1016/j.scitotenv.2014.09.079, 2015.

Zhang, W.C., Guo, J.P., Miao, Y.C., Liu, H., Song, Y., Fang, Z., He, J., Lou, M.Y., Yan, Y., Li, Y., Zhai, P.M., 2018. On the summertime planetary boundary layer with different thermodynamic stability in China: a radiosonde perspective. J. Clim. 31, 1451–1465.

Zhang, X., Cai, X., and Chai, F.: Structures and characteristics of the atmospheric boundary layer over Beijing area in autumn, Acta Sci. Natur. Univ. Pekinensis, 42, 220–225, 2006 (in Chinese).

Zhang, Y., & Li, Z. (2015). Remote sensing of atmospheric fine particulate matter (PM2.5) mass concentration near the ground from satellite observation. Remote Sensing of Environment, 160, 252-262.

Data availability. The lidar data used in this study can be requested from the corresponding author (lizq@radi.ac.cn).

Author contributions. ZL conceived and designed the study. JG collected and processed the radiosonde data. YL, HX and PG collected the lidar data. HW improved the MLH retrieval algorithm from lidar. HW processed and analyzed the data and prepared the manuscript.

Competing interests. The authors declare no competing interests.

Acknowledge. The authors acknowledge the assistance of acquisition of radiosonde data by Dr. Guo J. P.. The authors would like to acknowledge China Meteorological Administration for obtaining the radiosonde data in Beijing. The authors thank Dr. Tang G. Q. for helpful discussions on algorithm improvement. This work was supported by National Natural Science Foundation of China (Grant No. 41671367, No. 41925019) and the program of 305090306.

https://doi.org/10.5194/acp-2020-175
Preprint. Discussion started: 16 March 2020

Atmospheric Chemistry and Physics Discussions

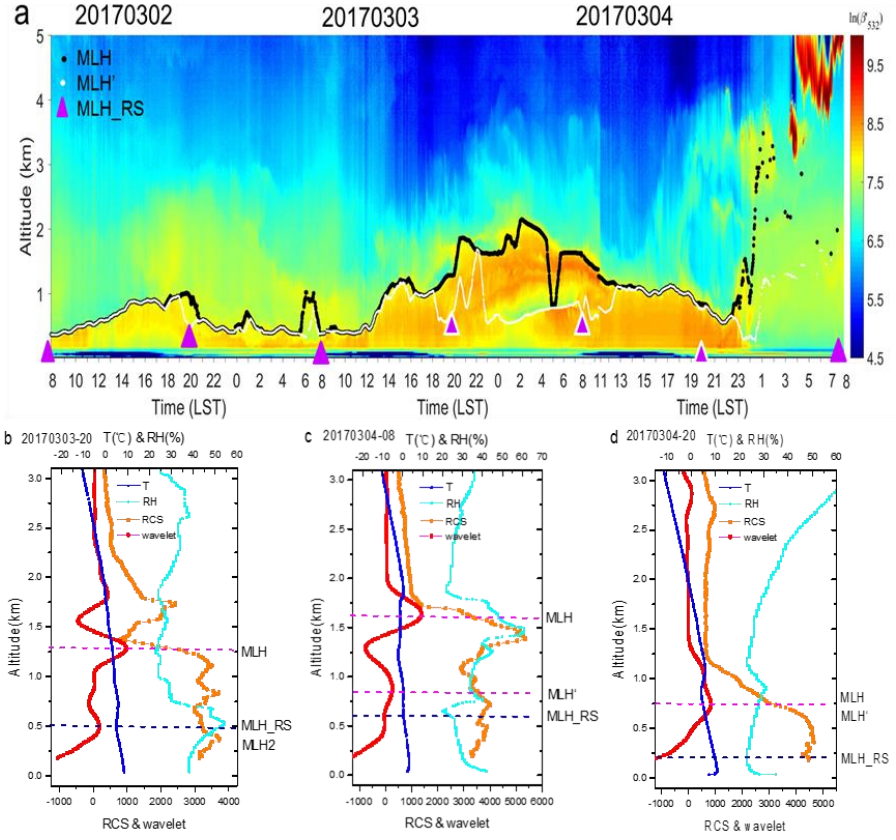

445 Fig. 1. Upper: (a) Daily backscatter profiles from lidar for 20170302-20170304 cases. The lines connected by black dots in the figure represent the retrieved MLH, while white dots line indicate the MLH' and purple triangle indicate the MLH identified from radiosonde. The horizontal axis represents the local standard time（LST） and the vertical axis represents the height. Colorbar denotes the logarithm of the attenuated backscattering coefficient (In(β'_{532})).

Lower: The vertical profile of RCS (orange curve) from lidar and wavelet coefficient (red curve) of RCS, as well as the vertical

450 profile of temperature (T) (blue curve) and relative humidity (RH) (cyan curve) for time of (b)20170303-20、(c)20170304-08 and (d)20170304-20 indicated by the white edge triangle in the upper picture (a).

https://doi.org/10.5194/acp-2020-175
Preprint. Discussion started: 16 March 2020

Atmospheric Chemistry and Physics Discussions

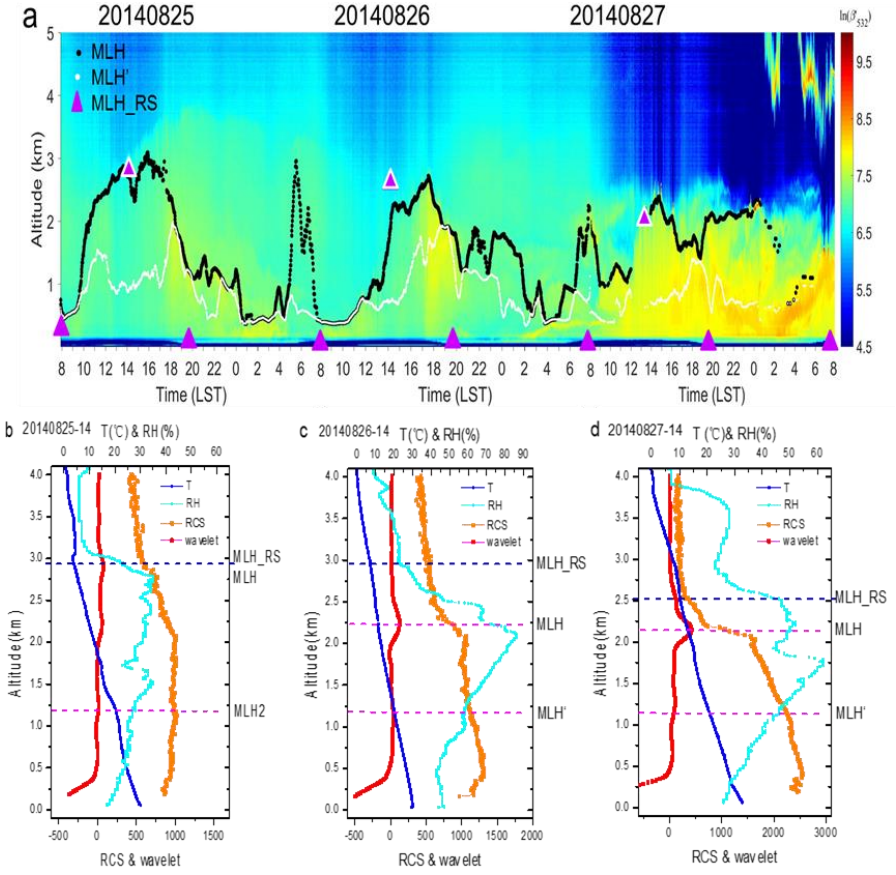

Fig.2. Similar as Fig.1, but for (a)20140825-20140827 case, and vertical profile for (b)20140825-14、(c)20140827-14 and

455 (d)20140827-20.

https://doi.org/10.5194/acp-2020-175
Preprint. Discussion started: 16 March 2020

Atmospheric Chemistry and Physics Discussions

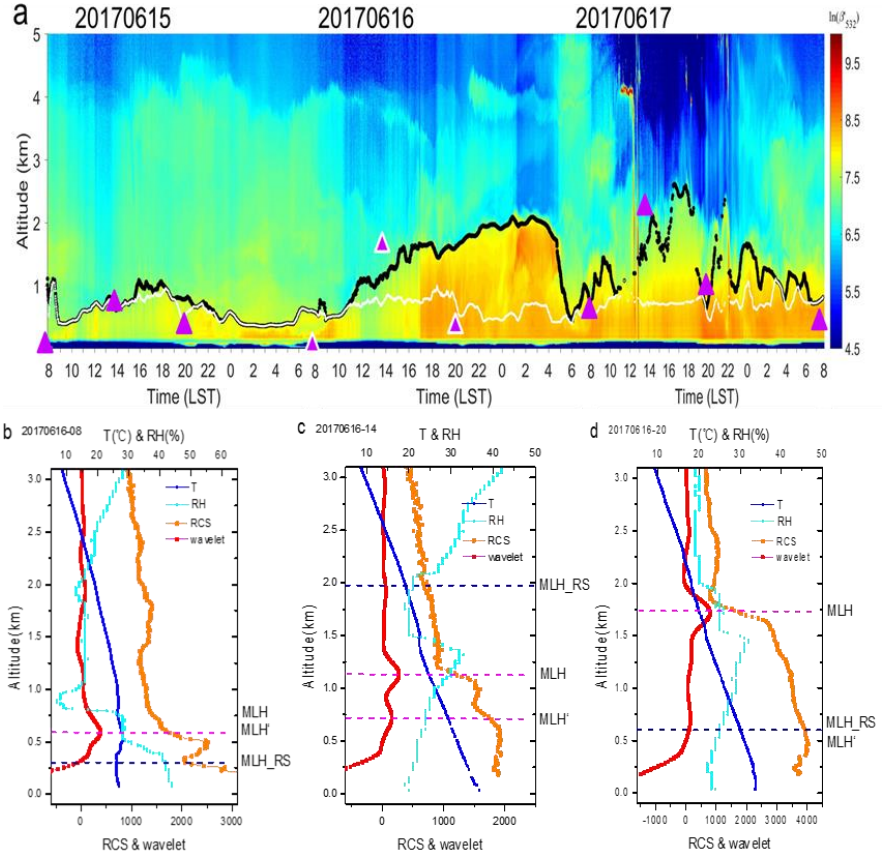

Fig.3. Similar as Fig.1, but for (a)20170615-20170617 case, and vertical profile for (b)20170616-08、(c)20170616-14 and (d)20170616-20.

https://doi.org/10.5194/acp-2020-175
Preprint. Discussion started: 16 March 2020

Atmospheric Chemistry and Physics Discussions

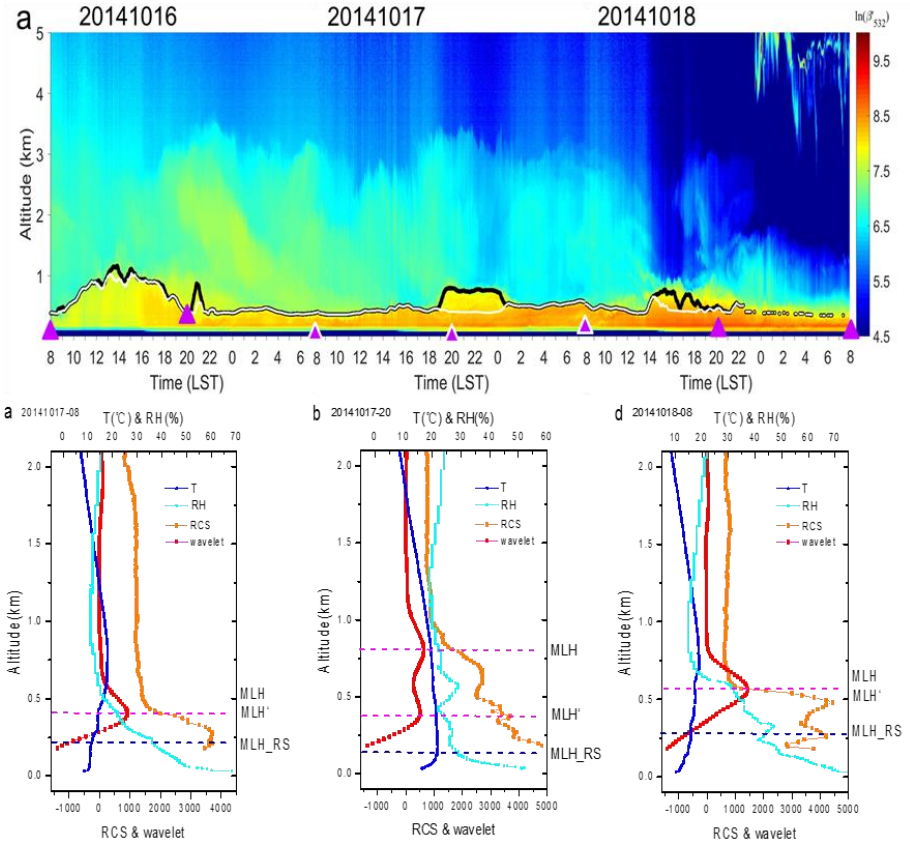

Fig.4. Similar as Fig.1, but for (a)20141016-20141018 case, and vertical profile for (b)20141017-08、(c)20141017-20 and (d)20141018-08.

https://doi.org/10.5194/acp-2020-175
Preprint. Discussion started: 16 March 2020

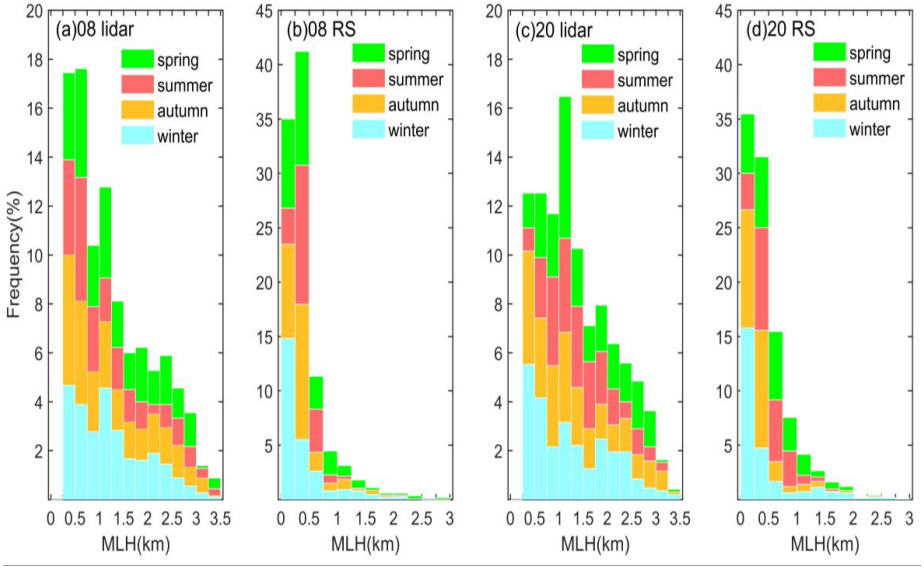

Fig.5. Comparison of frequency distribution of MLH retrieved from lidar and radiosonde for different seasons. MLH from (a) lidar and (b) radiosonde at time of 08 (LST), (c) lidar and (d) radiosonde at time of 20 (LST) are presented.

https://doi.org/10.5194/acp-2020-175
Preprint. Discussion started: 16 March 2020

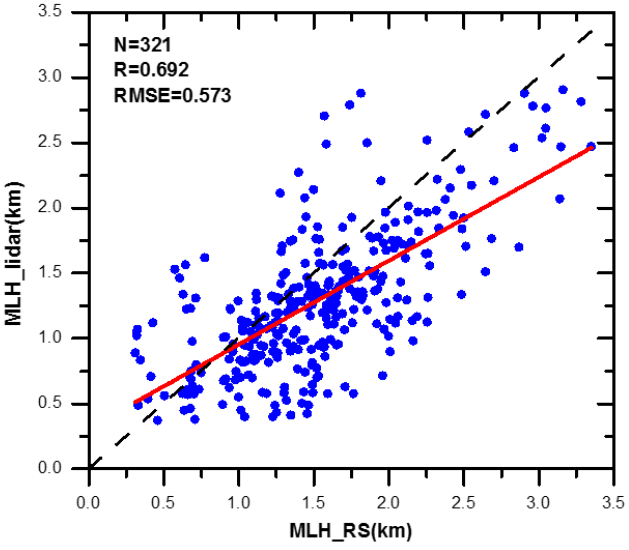

475 Fig.6. Comparisons between MLH in summer derived from lidar and from radiosonde at time of 14 (LST). Red line indicates the linear fitting of 321 samples, while the black dash line represents the 1:1 line.

https://doi.org/10.5194/acp-2020-175
Preprint. Discussion started: 16 March 2020

Atmospheric Chemistry and Physics Discussions

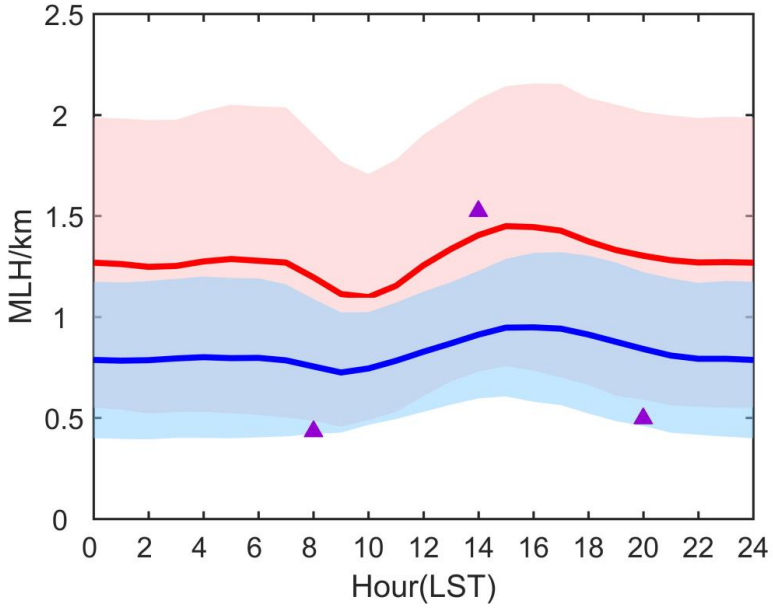

480 Fig. 7. Diurnal cycles of mixing layer height. The red line indicates the MLH retrieved from lidar, and the blue line represent the MLH' from lidar. The shaded areas show the standard deviation of MLH and MLH'. Purple triangles indicate the MLH averaged from routine RS data at 08 and 20 time (LST), and from summer radiosonde at time of 14 (LST).

https://doi.org/10.5194/acp-2020-175
Preprint. Discussion started: 16 March 2020

Atmospheric Chemistry and Physics Discussions

485

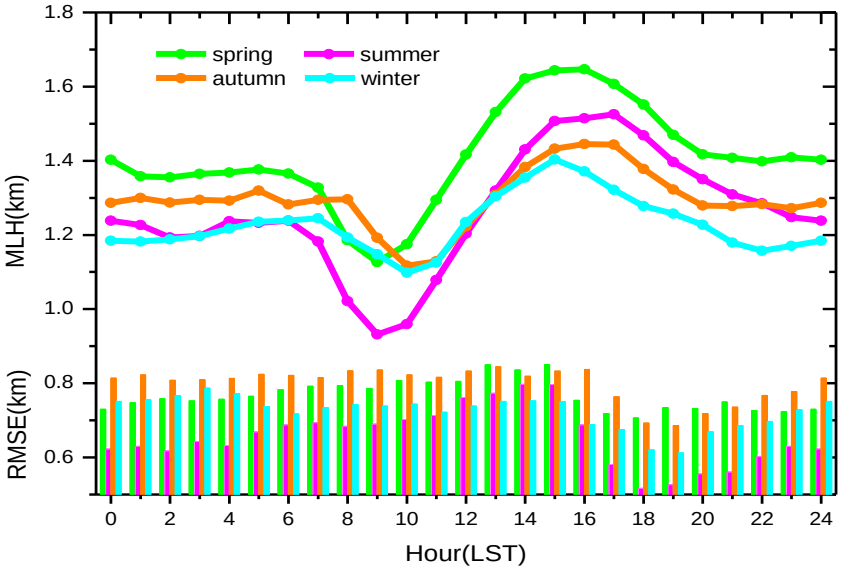

Fig. 8. Seasonal variation of diurnal cycles of MLH retrieved from lidar (dot lines), as well as the standard deviation of MLH（histograms）.

https://doi.org/10.5194/acp-2020-175
Preprint. Discussion started: 16 March 2020

Atmospheric Chemistry and Physics Discussions

490

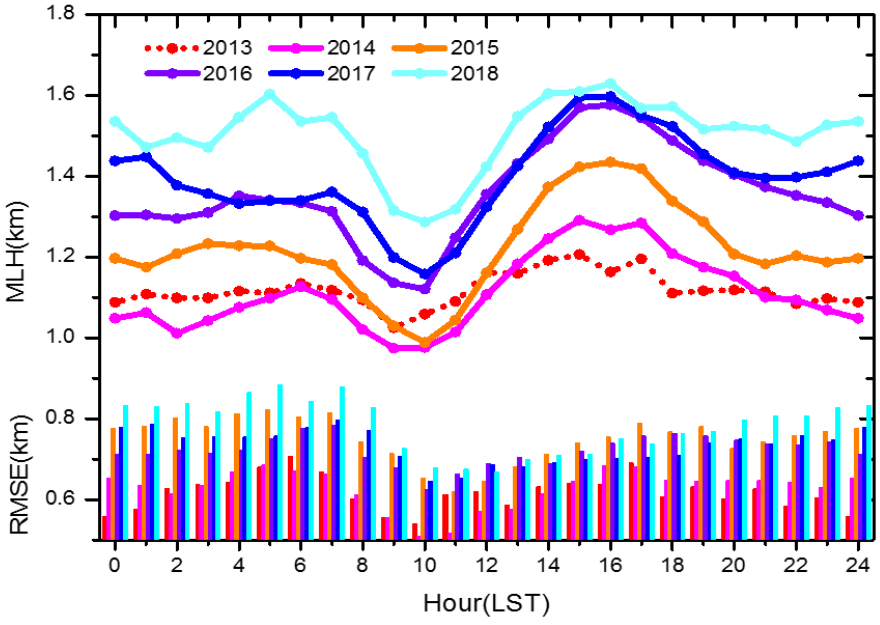

Fig. 9. Interannual variation of diurnal cycles of averaged MLH retrieved from lidar (dot lines), as well as the standard deviation of MLH (histograms).

https://doi.org/10.5194/acp-2020-175
Preprint. Discussion started: 16 March 2020

Atmospheric Chemistry and Physics Discussions

495

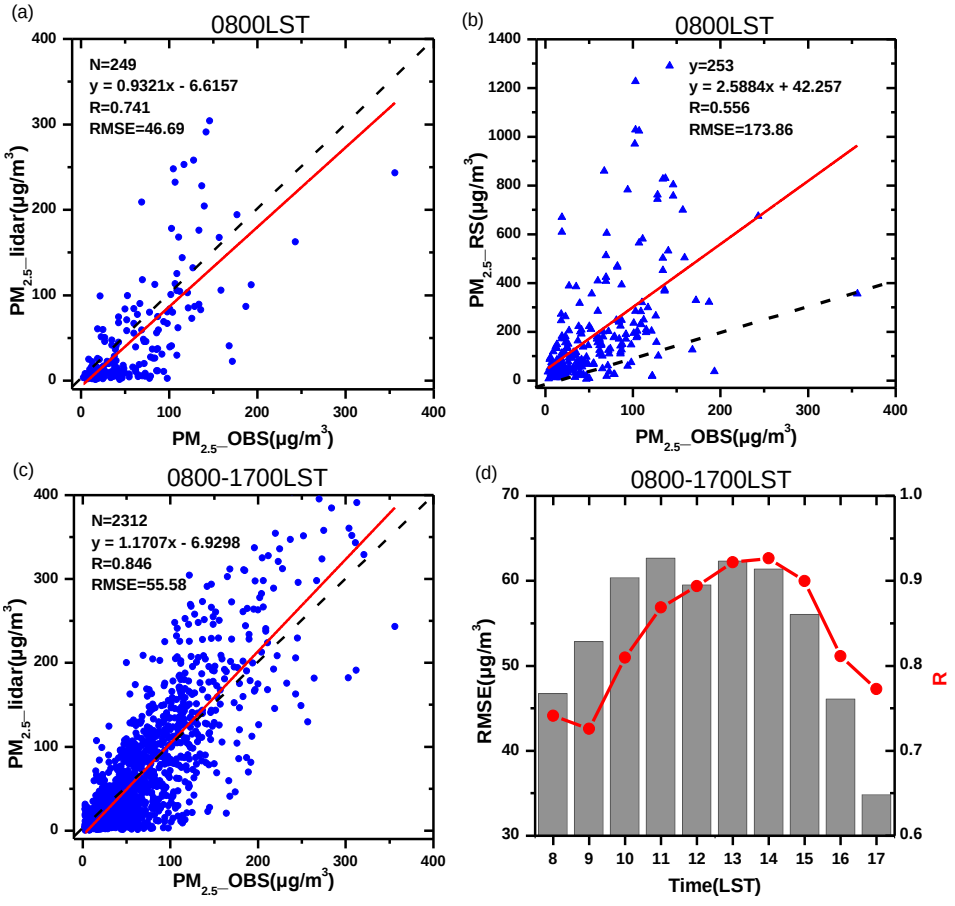

Fig.10. Comparisons between observed $PM_{2.5}$ and $PM_{2.5}$ calculated from PMRS model using (a) MLH_lidar and (b) MLH_RS at time of 0800(LST), and (c) MLH_lidar for the period of 0800-1700(LST) , and (d) correlation coefficient and standard deviation between observed $PM_{2.5}$ and $PM_{2.5}$ calculated from PMRS model using MLH_lidar for each hour
500 from 0800 to 1700 LST.